Results in Physics 54 (2023) 107084

Contents lists available at ScienceDirect

Results in Physics

journal homepage: www.elsevier.com/locate/rinp

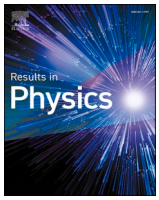

Fast and slow magnetosonic shock waves in non-Maxwellian plasmas

Navaira Izhar [a], M.N.S. Qureshi [a,*], J.K. Shi [b], H.A. Shah [c]

[a] Department of Physics, GC University, Lahore 54000, Pakistan
[b] State Key Laboratory of Space Weather, National Space Science Centre, Chinese Academy of Sciences, Beijing 100190, PR China
[c] Department of Physics, FC College (A Charted University), Lahore 54600, Pakistan

A B S T R A C T

Obliquely propagating nonlinear fast and slow magnetosonic wave modes in a hot non-Maxwellian dissipative plasma are investigated in the current work. Modified temperatures have been derived for the non-extensive Q- and (r,q)-distributions that correspond to the physical properties of such non-Maxwellian plasmas. The reductive perturbation technique has been employed to derive the linear dispersion relation (LDR) and Kadomstev-Petvashvilli-Burgers (KPB) equation for slow and fast magnetosonic wave modes in two dimensions. We then investigated the effect of non-extensive parameter Q, spectral indices (r,q) and kinematic viscosity ν on the LDR and nonlinear propagation of KPB shock profiles for both the slow and fast mode magnetosonic waves. We found that linear and nonlinear propagation of fast and slow magnetosonic wave modes have been considerably modified in such non-Maxwellian plasmas. The results presented here would depict a realistic picture of the propagation of linear and nonlinear fast and slow magnetosonic wave modes in non-Maxwellian plasmas.

Introduction

A significant amount of research has been carried out since the discovery of magnetosonic waves in the fields of observations, theoretical investigations and simulations [1–9]. In the magnetohydrodynamic (MHD) picture, fast and slow modes of magnetosonic waves are the fundamental low frequency modes in magnetized plasma [10–13]. In addition to these low frequency modes, in ideal MHD when heat conduction is added, there are two other roots as well, called entropy modes, characterized by non-propagating perturbations of thermodynamical properties of plasma with almost zero frequency [14]. Propagation of magnetosonic solitary waves has been the subject of interest for many researchers due to their importance in particle acceleration and heating in fusion devices, space and astrophysical plasmas. Boardsen et al. [2] observed the fast magnetosonic waves at large angles to the ambient magnetic field at the magnetic equator associated with the proton ring distributions. In the Earth's magnetosphere, Horne et al. [3] investigated the generation, growth and decay of radially propagating fast magnetosonic waves and found that protons are heated as a result of these waves. Fast magnetosonic waves have also been found to be responsible for electron heating and are thought to play an important role in the dynamics of radiation belts [4]. Intense magnetosonic waves have been observed in the plasma sphere associated with the proton ring distributions which provide the free energy for their excitations [5].

Shah and Bruno [1] investigated obliquely propagating fast and slow magnetosonic modes in a hot plasma and derived the Kadomstev-Petvashvilli (KP) equation for arbitrary plasma beta. Mushtaq and Shah [10] studied nonlinear magnetosonic waves propagating obliquely to the external magnetic field in electron–positron-ion (*epi*) plasma and considered the effect of plasma beta on the propagation of fast and slow modes. Chakrborty and Das [11] studied the effect of finite Larmor radius on the oblique propagation of magnetosonic waves and where it was shown that these waves are governed by KP equation in a collisionless plasma with an additional dispersive term. Magnetosonic waves have also been studied using quantum-hydrodynamic (QHD) model in a dense plasma and where both the hump and dip soliton structures, were investigated for various plasma parameters [12]. The KP and cylindrical Kadomtsev-Petviashili-Burgers (CKPB) equations have been derived for nonlinear magnetosonic waves in quantum dusty magnetized plasmas [15,16].

In theoretical studies on the nonlinear magnetosonic waves mentioned above, collisions have been ignored which may occur between neutrals and charged particles as well as between charged particles [13]. Due to collisions (or any kind of dissipation) in various laboratory and space plasmas, the nonlinear evolution of magnetosonic waves modifies significantly. In a collisional plasma, one-dimensional propagation of magnetosonic waves has been governed by Korteweg-de Vries-Burger's (KdV-B) equation [17]. In a two-dimensional warm collisional plasma, obliquely propagating magnetosonic waves have been governed by Kadomstev-Petvashvilli-Burger's (KPB) equation [18,19]. In a dusty of inertialess electrons and ions and here it is shown that these waves are governed by the modified Korteweg-de Vries

* Corresponding author.
E-mail address: noumansarwar@gcu.edu.pk (M.N.S. Qureshi).

https://doi.org/10.1016/j.rinp.2023.107084
Received 8 July 2023; Received in revised form 24 September 2023; Accepted 12 October 2023
Available online 15 October 2023

(mKdV) equation [20]. Later, dissipative structures have been obtained by studying nonlinear magnetosonic waves in a pair-ion plasma in the presence of ion–electron collisions [21]. Considering ion-neutral collisions, the damped Korteweg-de Vries (DKdV) equation has been obtained for perpendicularly propagating magnetosonic waves and characteristics of damped soliton structures were examined [22–23].

Distribution function and modified temperature

It is well known that space plasmas are tenuous and collisionless, therefore observations of distribution functions from various regions including solar wind and Earth's magnetosphere, generally exhibit nonthermal features such as high energy tail [24–27] and flat top or spiky nature at low energies [28–31]. Distributions with high energy tail and Gaussian peak are well modeled with power law kappa (κ) distribution function, where κ index measures the strength of the high energy tail. For $\kappa \to \infty$, the distribution approaches a Maxwellian. However, when the observed distributions exhibit flat top or spike at low energies, the double spectral index distribution, i.e. the generalized (r,q) distribution function becomes the ultimate choice [32]. In the limiting cases, $r=0, q\to\infty$ and $r=0, q\to(\kappa+1)$, Maxwellian and kappa distributions can be recovered from (r,q) distribution, respectively. Recently, (r,q) distribution has been employed in numerous studies and the results have shown that these are significantly improved both qualitatively and quantitatively [33–38]. Thus (r,q) distribution has stimulated new avenues for studying the linear and nonlinear waves which are significantly different from the standard Maxwellian and power law distributions. The three-dimensional (r,q) distribution function has the form

$$f_{rq}(v) = \frac{3\Gamma(q)(q-1)^{-3/(2+2r)}}{4\pi(A2T/m)^{3/2}\Gamma\left(q-\frac{3}{2+2r}\right)\Gamma\left(1+\frac{3}{2+2r}\right)}\left(1+\frac{1}{q-1}\left[\frac{v^2}{V_{th}^2}\right]^{1+r}\right)^{-q} \tag{1}$$

where

$$A = \frac{3(q-1)^{-1/(1+r)}\Gamma\left(\frac{3}{2+2r}\right)\Gamma\left(q-\frac{3}{2+2r}\right)}{2\Gamma\left(\frac{5}{2+2r}\right)\Gamma\left(q-\frac{5}{2+2r}\right)} \tag{2}$$

and $V_{th}=\sqrt{A(2k_BT)/m}$ is the modified thermal velocity, Γ is the gamma function, m is the particle's mass, T is the particle's temperature in thermal equilibrium and k_B is the Boltzmann constant.

In recent times, there has been an increasing trend to use another power law distribution which is based on Tsallis statistics, known as non-extensive Q-distribution, which in the limit $Q\to1$ reduces to Maxwellian distribution [39]. The non-extensive Q-distribution also shows flat top as well as Gaussian peak at low energies similar to (r,q) distribution, that is why we are going to employ both of these distributions in our study and present a comparison between these two. The three-dimensional non-extensive Q-distribution has the form [40–42]

$$f_Q(v) = B\left(1-[Q-1]\frac{v^2}{v_{th}^2}\right)^{\frac{1}{Q-1}} \tag{3}$$

where

$$B = \frac{\Gamma\left(\frac{1}{1-Q}\right)}{\Gamma\left(\frac{1}{1-Q}-\frac{3}{2}\right)}\left[\frac{1-Q}{\pi v_{th}^2}\right]^{3/2} \text{ for } \frac{1}{3} < Q \le 1 \tag{4}$$

$$B = \frac{3Q-1}{2}\frac{\Gamma\left(\frac{1}{Q-1}+\frac{3}{2}\right)}{\Gamma\left(\frac{1}{Q-1}\right)}\left[\frac{Q-1}{\pi v_{th}^2}\right]^{3/2} \text{ for } Q \ge 1 \tag{5}$$

and $v_{th}=\sqrt{(2k_BT)/m}$ is the thermal velocity. In Fig. 1, we plot the (r,q) and non-extensive Q-distributions for different values of spectral indices r,q and Q-parameter. From Fig. 1(a), we can see that for $Q<1$ and $r<0$, both the distributions exhibit excess of superthermal particles with a Gaussian peak for Q-distribution and spiky peak for (r,q) distribution. However, for $Q>1$, the Q-distribution exhibits smaller number of high energy particles as compared to the Maxwellian distribution and for $r>0$, the (r,q) distribution exhibits flat top or shoulders at low velocities which becomes more prominent as r increases (Fig. 1(b)). For comparison, kappa and Maxwellian distributions are also given in Fig. 1.

In most of the earlier studies, fluid treatment of magnetosonic waves was based on the assumption that the plasma is in thermal equilibrium and the pressure can be calculated by the ideal gas equation $p=nk_BT$, where n is the total number density and T is the particle's temperature. In the context of kinetic theory, pressure is defined as $p=\frac{1}{3}nm<v^2>$, where $<v^2>$ is the mean square velocity of the particle, given as $<v^2>=\frac{1}{n}\int f(v)d^3v$. The mean square velocity of the particle for the cases of (r,q) and non-extensive Q-distribution can thus be calculated, respectively, as [42–43]

$$<v^2>_{rq} = \frac{(q-1)^{\frac{1}{1+r}}\Gamma\left(\frac{5}{2+2r}\right)\Gamma\left(q-\frac{5}{2+2r}\right)}{\Gamma\left(\frac{3}{2+2r}\right)\Gamma\left(q-\frac{3}{2+2r}\right)}\frac{2k_BT}{m} \tag{6}$$

and

$$<v^2>_Q = \frac{3}{5Q-3}\frac{2k_BT}{m} \tag{7}$$

We can note that the standard expression of mean square velocity can be recovered from the above Eqs. (6) and (7) in the limits $r=0, q\to\infty$ and $Q\to1$, respectively. Thus the ideal gas equation for the cases of (r,q) and non-extensive Q-distributions can be written as

$$p_{rq} = \frac{1}{3}nm<v^2>_{rq} = \frac{1}{3}nm\frac{(q-1)^{\frac{1}{1+r}}\Gamma\left(\frac{5}{2+2r}\right)\Gamma\left(q-\frac{5}{2+2r}\right)}{\Gamma\left(\frac{3}{2+2r}\right)\Gamma\left(q-\frac{3}{2+2r}\right)}\frac{2k_BT}{m} = nk_BT_{rq} \tag{8}$$

$$p_Q = \frac{1}{3}nm<v^2>_Q = \frac{1}{3}nm\frac{3}{5Q-3}\frac{2k_BT}{m} = nk_BT_Q \tag{9}$$

where

$$T_{rq} = \frac{2(q-1)^{\frac{1}{1+r}}\Gamma\left(\frac{5}{2+2r}\right)\Gamma\left(q-\frac{5}{2+2r}\right)}{3\Gamma\left(\frac{3}{2+2r}\right)\Gamma\left(q-\frac{3}{2+2r}\right)}T \tag{10}$$

and

$$T_Q = \frac{2}{5Q-3}T \tag{11}$$

are the modified temperatures representing the (r,q)-distributed and Q-distributed plasmas, whereas T is the temperature representing the system in thermal equilibrium. In the limit $Q\to1$, T_Q approaches to T [43–46], for $r=0, q\to(\kappa+1)$, T_{rq} becomes $T_\kappa=\frac{2\kappa}{2\kappa-3}T$ which is the modified temperature for κ-distributed plasma 46–48 and for $r=0$, $q\to\infty$, T_{rq} becomes T. It should be noted that to keep T_Q, T_{rq} and T_κ

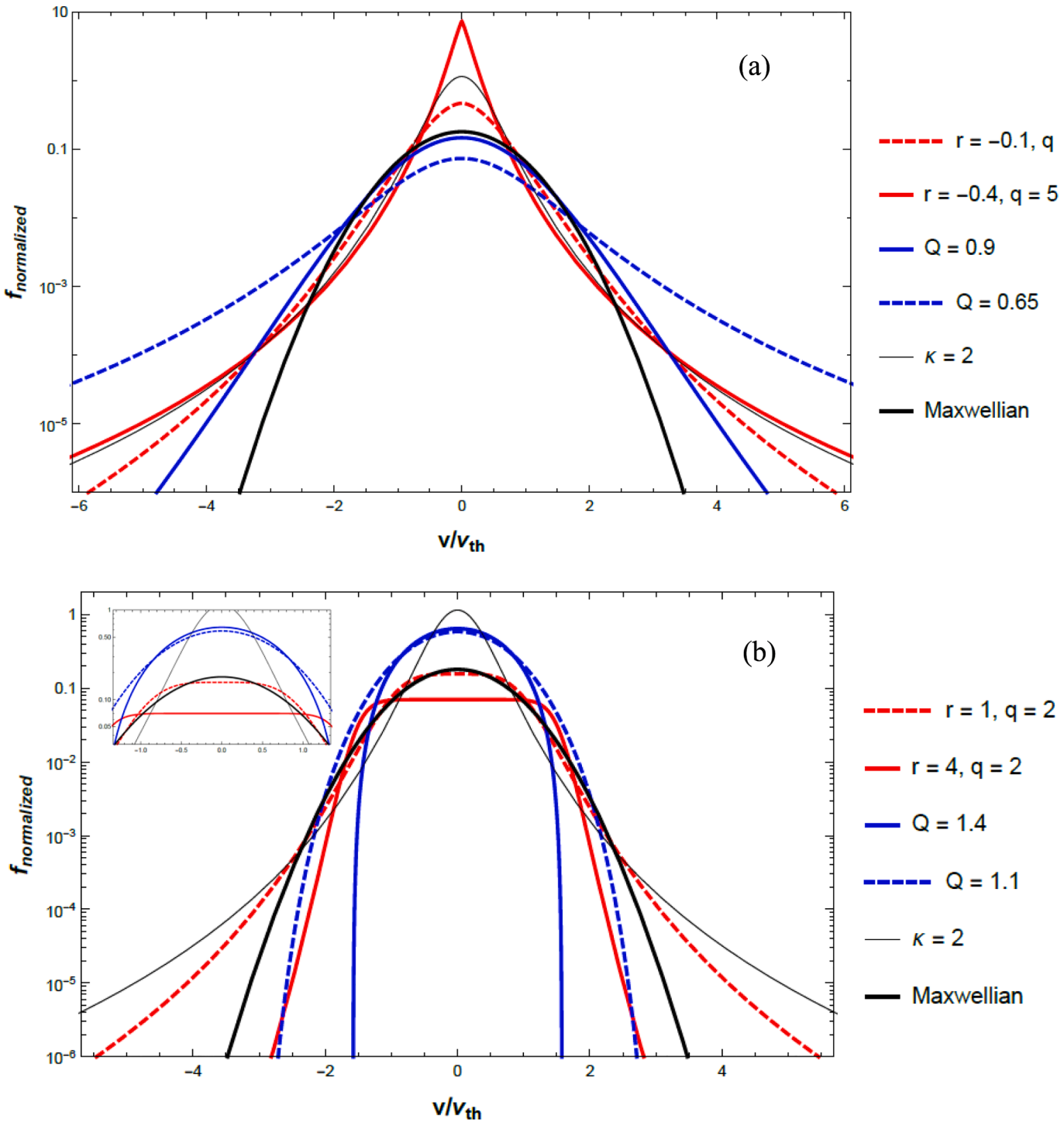

Fig. 1. Non-extensive Q-distribution (blue lines), (r,q)-distribution (red lines) and limiting forms of (r,q)-distribution, i.e. kappa (black thin line) and Maxwellian (black bold line) distributions for (a) $Q<1$ and $r<0$ and (b) $Q>1$ and $r>0$. (For interpretation of the references to colour in this figure legend, the reader is referred to the web version of this article.)

positive, conditions $Q>3/5$, $q>1 \text{and} q(r+1)>5/2$, and $\kappa>3/2$, respectively, should be satisfied [28 43,47].

To the best of the author's knowledge, obliquely propagating magnetosonic wave in a hot, dissipative nonthermal plasma has never been studied by deriving Kadomstev-Petvashvilli-Burger (KPB) equation. Hence, in this paper, we study the linear and nonlinear propagation of slow and fast magnetosonic wave modes in nonthermal plasma and derive the KPB equation. The effects of modified temperatures are investigated on the linear and nonlinear propagation of both the slow and fast magnetosonic wave modes. The foremost aim of this paper is to present the set of nonlinear equations for the hot, dissipative nonthermal plasma by incorporating the different nonthermal distributions, which would be used to describe the two-dimensional magnetosonic waves and provide the basis for future study.

Basic equations

We consider a magnetized plasma in which the ambient magnetic

field $\boldsymbol{B}_0$ lies in the (x,y) plane making an angle θ with the x-axis and propagation in the (x,z) plane with propagation vector $\boldsymbol{k}$ making an angle φ with the x-axis. In order to derive the KPB equation, we write the one-fluid magnetohydrodynamic (MHD) equations for an isotropic, isothermal non-Maxwellian plasma [1,49–50]. The mass conservation equation is

$$\frac{\partial \rho}{\partial t} + \nabla.(\rho \boldsymbol{v}) = 0 \tag{12}$$

Equations of motion for ions and electrons, respectively, are

$$m_i n_i \frac{d\boldsymbol{v_i}}{dt} = n_i e\boldsymbol{E} + \frac{e}{c} n_i (\boldsymbol{v_i} \times \boldsymbol{B}) - \nabla p_i + \lambda \nabla^2 \boldsymbol{v_i} \tag{13}$$

$$m_e n_e \frac{d\boldsymbol{v_e}}{dt} = -n_e e\boldsymbol{E} - \frac{e}{c} n_e (\boldsymbol{v_e} \times \boldsymbol{B}) - \nabla p_e \tag{14}$$

By considering electrons as inertialess ($m_e = 0$) and using the quasi-neutrality condition $n_i \approx n_e$, above Eqs. (13) and (14) can be solved to get the one fluid equation of motions as

$$\rho \frac{d\boldsymbol{v}}{dt} = \frac{1}{c}(\boldsymbol{j} \times \boldsymbol{B}) - \nabla p_e + \lambda \nabla^2 \boldsymbol{v_i} \tag{15}$$

In the above equation, we considered $\nabla p_i = 0$ for $T_i \ll T_e$ which is true for most of the space plasmas, $\boldsymbol{v} = \boldsymbol{v_i}$ is the hydrodynamic velocity, $\boldsymbol{j} = en(\boldsymbol{v_i} - \boldsymbol{v_e})$, $m_i + m_e \approx m_i$, $\rho = m_i n_i$, $p_e = nk_B T_\alpha$ is the pressure where $\alpha = rq, Q$ and $\frac{d}{dt} = \left(\frac{\partial}{\partial t} + \boldsymbol{v}.\nabla\right)$.

Now multiply Eq. (13) by m_i and Eq. (14) by m_e and subtracting Eq. (14) by Eq. (13), and neglecting the $\frac{d}{dt}$ for slow motions where inertial effects are unimportant, we obtain the generalized Ohm's law as

$$\boldsymbol{E} = -\frac{\boldsymbol{v} \times \boldsymbol{B}}{c} + \frac{m_i}{4\pi \rho e} \boldsymbol{j} \times \boldsymbol{B} - \frac{m_i}{\rho e} \nabla p_e + \frac{m_i \lambda \nabla^2 \boldsymbol{v_i}}{\rho e} \tag{16}$$

The Maxwell's curl equations are

$$\nabla \times \boldsymbol{E} = -\frac{1}{c} \frac{\partial \boldsymbol{B}}{\partial t} \tag{17}$$

$$\nabla \times \boldsymbol{B} = \frac{4\pi}{c} \boldsymbol{J} \tag{18}$$

Upon using Eq. (18) into (15), we obtain

$$\frac{d\boldsymbol{v}}{dt} = \frac{1}{\rho}(\nabla \times \boldsymbol{B}) \times \boldsymbol{B} - \frac{\beta'}{\rho} \nabla p_e + \lambda \nabla^2 \boldsymbol{v_i} \tag{19}$$

By eliminating $\boldsymbol{E}$ from Eq. (16) using (17), we get

$$\frac{\partial \boldsymbol{B}}{\partial t} = \nabla \times (\boldsymbol{v} \times \boldsymbol{B}) - \frac{1}{\rho} \nabla \times [(\nabla \times \boldsymbol{B}) \times \boldsymbol{B}] \tag{20}$$

In the above Eqs. (12), (19) and (20), normalizations are taken as: $v = v/v_A$, $B = B/B_o$, $\rho = \rho/\rho_0$, $p = P/p_o$, $\nabla = \nabla(\frac{\Omega_i}{v_A})$, $t = t/_{\Omega_i^{-1}}$, $\lambda = \lambda(\frac{\Omega_i}{v_A^2})$ is the kinematic viscosity, where $\rho_0 = m_i n_0$, $\Omega_i = \frac{eB_o}{m_i c}$ and $\nabla^2 = \left(\frac{\partial^2}{\partial x^2} + \frac{\partial^2}{\partial z^2}\right)$. We note that $\beta'(= c_s'^2/v_A^2)$ contains all the nonthermal features, where $c_s' = (T_\alpha/m_i)^{1/2}$ is the modified acoustic speed, T_α is the modified temperature given in Eqs. (10) and (11), and $v_A = B_0/\sqrt{4\pi\rho_0}$ is the Alfven speed.

Derivation of KPB equation

Linear dispersion relation

Using the standard reductive perturbation method [1,51–53], we derive the KPB equation to study nonlinear magnetosonic waves propagating in two dimensions. We expand the various fluctuating quantities in dimensionless form with respect to small quantity ϵ, that measures the weakness of nonlinearity, as

$$\begin{aligned}
\rho &= 1 + \epsilon\rho_1 + \epsilon^2\rho_2 + \cdots \\
v_x &= \epsilon v_{x1} + \epsilon^2 v_{x2} + \cdots \\
v_y &= \epsilon v_{y1} + \epsilon^2 v_{y2} + \cdots \\
v_z &= \epsilon^{\frac{3}{2}} v_{z1} + \epsilon^{\frac{5}{2}} v_{z2} + \cdots \\
B_x &= \cos\theta \\
B_y &= \sin\theta + \epsilon B_{y1} + \epsilon^2 B_{y2} + \cdots \\
B_z &= \epsilon^{\frac{3}{2}} B_{z1} + \epsilon^{\frac{5}{2}} B_{z2} + \cdots
\end{aligned} \tag{21}$$

and the stretched variables are introduced, as

$$\begin{aligned}
\xi &= \epsilon^{\frac{1}{2}}(x - Vt) \\
\eta &= \epsilon z \\
\tau &= \epsilon^{\frac{3}{2}} t \\
\lambda &= \epsilon^{\frac{1}{2}} \nu
\end{aligned} \tag{22}$$

where $V = V_p/v_A$ is the normalized phase velocity.

Upon using Eqs. (21) and (22) into set of Eqs. (12) to (20), and equating terms in lowest order of ϵ, we obtain the first order equations as

$$\begin{aligned}
V\frac{\partial \rho_1}{\partial \xi} - \frac{\partial v_{x1}}{\partial \xi} &= 0 \\
V\frac{\partial v_{x1}}{\partial \xi} &= \beta'\frac{\partial \rho_1}{\partial \xi} + \sin\theta \frac{\partial B_{y1}}{\partial \xi} \\
V\frac{\partial v_{y1}}{\partial \xi} &= -\cos\theta \frac{\partial B_{y1}}{\partial \xi} \\
V\frac{\partial B_{y1}}{\partial \xi} &= \sin\theta \frac{\partial v_{x1}}{\partial \xi} - \cos\theta \frac{\partial v_{y1}}{\partial \xi}
\end{aligned} \tag{23}$$

From the above set of Eqs. (23), we obtain the linear quantities, as

$$\begin{aligned}
v_{x1} &= \left(\frac{V\sin\theta}{(V^2 - \beta')}\right) B_{y1} \\
v_{y1} &= \left(\frac{\cos\theta}{V}\right) B_{y1} \\
\rho_1 &= \left(\frac{\sin\theta}{(V^2 - \beta')}\right) B_{y1}
\end{aligned} \tag{24}$$

which results in linear dispersion relation (LDR) for magnetosonic waves propagating in two dimensions, as

$$V^2 = \frac{1 + \beta'}{2}\left[1 \pm \left(1 - \frac{4\beta' cos^2\theta}{(1 + \beta')^2}\right)^{\frac{1}{2}}\right] \tag{25}$$

In the above LDR, fast magnetosonic mode in the super Alfvenic regime is represented by the upper sign (+) and slow magnetosonic mode in the sub-Alfvenic regime is represented by the lower sign (-). It should be noted that if $\theta = 90^\circ$ and the propagation is considered along x-axis, i.e. $\varphi = 0$ in Eq. (25), LDR represents the pure magnetosonic wave for the case of fast mode. However, if $\theta = 0^\circ$ and the propagation is again considered along x-axis, i.e. $\varphi = 0$ in Eq. (25), LDR represents the pure Alfven wave for the fast mode and represents sound waves for the slow mode.

Fig. 2 depicts the linear phase velocity $V = V_p/v_A$ against the angle θ for fast mode (FM) as well as slow mode (SM) for non-extensive Q-distribution, (r,q)-distribution and limiting forms of (r,q)-distribution, i.e. kappa and Maxwellian distributions. Fig. 2(a) and 2(b) are plotted for $Q < 1$ and $r < 0$, in which we can see that phase velocity for FM increases but for SM decreases with θ. We can also note that for the FM (Fig. 2(a)) as well as for the SM (Fig. 2(b)), the phase velocity is highest

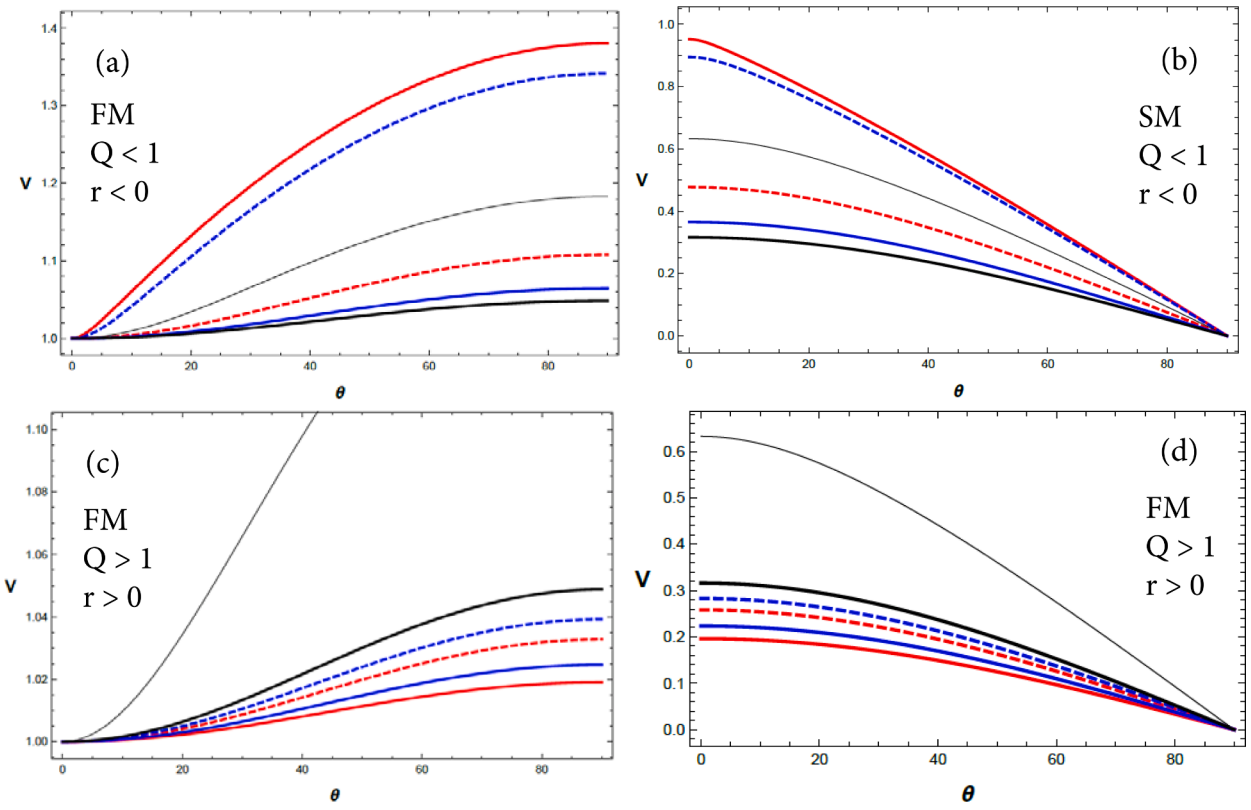

Fig. 2. (a) and (b) depict the linear phase velocity V vs. θ for fast and slow modes, respectively, when $Q = 0.65$ (dashed blue line), $Q = 0.9$ (solid blue line), $r = -0.1, q = 5$ (dashed red line), $r = -0.31, q = 5$ (solid red line). (c) and (d) depict the linear phase velocity V vs. θ for fast and slow modes, respectively, when $Q = 1.1$ (dashed blue line), $Q = 1.4$ (solid blue line), $r = 1, q = 2$ (dashed red line), $r = 4, q = 2$ (solid red line). In Fig. 2(a)-(d), thin black line represents kappa distribution ($\kappa = 2$) and bold black line represents Maxwellian distribution. (For interpretation of the references to colour in this figure legend, the reader is referred to the web version of this article.)

for (r, q)-distribution ($r = -0.31, q = 5$) exhibiting maximum spiky distribution with high energy tail and least for Maxwellian (Fig. 2(a) and 2(b)). Fig. 2(c) and (d) are plotted for $Q > 1$ and $r > 0$, in which for the FM we can see that phase velocity increases with θ but for SM it decreases with θ. We can also note that for the FM (Fig. 2(c) as well as for the SM (Fig. 2(d)), the phase velocity is highest for κ-distribution ($\kappa = 2$) exhibiting maximum high energy tail and least for (r, q)-distribution ($r = 4, q = 2$) showing broader shoulders at low energies.

Nonlinear treatment

In order to develop KP equation for both slow and fast modes, we write the ϵ^2 and $\epsilon^{5/2}$ order terms using Eqs. (11) and (12) into Eqs. (1), (9) and (10), respectively, and get

$$V\frac{\partial v_{z1}}{\partial \xi} = \sin\theta\frac{\partial B_{y1}}{\partial \eta} - \cos\theta\frac{\partial B_{z1}}{\partial \xi} + \beta'\frac{\partial \rho_1}{\partial \eta}$$
$$V\frac{\partial B_{z1}}{\partial \xi} = -\cos\theta\frac{\partial v_{z1}}{\partial \xi} + \cos\theta\frac{\partial^2 B_{y1}}{\partial \xi^2} \tag{26}$$

and

$$\frac{\partial \rho_1}{\partial \tau} + \rho_1\frac{\partial v_{x1}}{\partial \xi} + v_{x1}\frac{\partial \rho_1}{\partial \xi} + \frac{\partial v_{z1}}{\partial \eta} = V\frac{\partial \rho_2}{\partial \xi} - \frac{\partial v_{x2}}{\partial \xi}$$
$$\frac{\partial v_{x1}}{\partial \tau} + v_{x1}\frac{\partial v_{x1}}{\partial \xi} - \beta'\rho_1\frac{\partial \rho_1}{\partial \xi} + B_{y1}\frac{\partial B_{y1}}{\partial \xi} - \rho_1\sin\theta\frac{\partial B_{y1}}{\partial \xi}$$
$$= V\frac{\partial v_{x2}}{\partial \xi} - \beta'\frac{\partial \rho_2}{\partial \xi} - \sin\theta\frac{\partial B_{y2}}{\partial \xi}$$
$$\frac{\partial v_{y1}}{\partial \tau} + v_{x1}\frac{\partial v_{y1}}{\partial \xi} + \cos\theta\rho_1\frac{\partial B_{y1}}{\partial \xi} - \nu\frac{\partial^2 v_{y1}}{\partial \xi^2} = V\frac{\partial v_{y2}}{\partial \xi} + \cos\theta\frac{\partial B_{y2}}{\partial \xi} \tag{27}$$
$$\frac{\partial B_{y1}}{\partial \tau} + B_{y1}\frac{\partial v_{x1}}{\partial \xi} + B_{u1}\frac{\partial B_{y1}}{\partial \xi} + \sin\theta\frac{\partial v_{z1}}{\partial \eta} - \cos\theta\frac{\partial^2 B_{z1}}{\partial \xi^2}$$
$$= V\frac{\partial B_{y2}}{\partial \xi} + cos\theta\frac{\partial v_{y2}}{\partial \xi} - \sin\theta\frac{\partial v_{x2}}{\partial \xi}$$

From the Eqs. (14) and (17), we get the following equations.

$$\frac{\partial B_{z1}}{\partial \xi} = \frac{V^2\cos\theta\sin\theta}{(\cos^2\theta - V^2)(V^2 - \beta')}\frac{\partial B_{y1}}{\partial \eta} - \frac{V\cos\theta}{(\cos^2\theta - V^2)}\frac{\partial^2 B_{y1}}{\partial \xi^2} \tag{28}$$

$$\frac{\partial v_{z1}}{\partial \xi} = -\frac{V^3 sin\theta}{(\cos^2\theta - V^2)(V^2 - \beta')}\frac{\partial B_{y1}}{\partial \eta} + \frac{\cos^2\theta}{(\cos^2\theta - V^2)}\frac{\partial^2 B_{y1}}{\partial \xi^2} \tag{29}$$

Rather monotonous but simple algebraic operations leads to the following KPB equation.

$$\frac{\partial}{\partial \xi}\left[\frac{\partial B_{y1}}{\partial \tau} + CB_{y1}\frac{\partial B_{y1}}{\partial \xi} - D\frac{\partial^2 B_{y1}}{\partial \xi^2} + E\frac{\partial^3 B_{y1}}{\partial \xi^3}\right] + F\frac{\partial^2 B_{y1}}{\partial \eta^2} = 0 \tag{30}$$

where, $C = b/a$, $D = c/a$, $E = d/a$, $F = e/a$, and

$$a = \frac{1}{V^2\left(V^2-\beta^{'}\right)^2}\left[V^6+V^4(1-2\beta^{'})+V^2\beta^{'}\left(1-3\cos^2\theta+\beta^{'}\right)+\beta^{'^2}\cos^2\theta\right]$$

$$b = \frac{\sin\theta}{\left(V^2-\beta^{'}\right)^3}\left[3V^5-V\beta^{'}\left(6V^2-3\beta^{'}-2\sin^2\theta\right)\right]$$

$$c = \frac{-V^4+\beta^{'}\left(2V^2-\beta^{'}\right)\cos^2\theta}{V^2\left(V^2-\beta^{'}\right)^2}\nu$$

$$d = \frac{V\cos^2\theta}{\left(\cos^2\theta-V^2\right)}$$

$$e = \frac{V^5\sin^2\theta}{\left(V^2-\cos^2\theta\right)\left(V^2-\beta^{'}\right)^2}$$

Equation (30) is a nonlinear partial differential equation that contains both dispersion and dissipation for which the most efficient and convenient method to solve such equation is the tanh method [53–55]. In our model, we considered viscosity, however, if we add collisions in our model we get non-stationary solutions, e.g. Raut et al. [56] derived the damped forced KP equation using the reductive perturbation method to obtain the non-stationary solitary solution for ion acoustic waves. Therefore, the solution of Eq. (30) using the tanh method, can be written as [57]

$$B_y = \frac{6D^2}{25CE}\left[1-tanh\left(\frac{D}{10E}\chi\right)\right]+\frac{3D^2}{25CE}\left[sech^2\left(\frac{D}{10E}\chi\right)\right] \tag{31}$$

where we have assumed $B_y = B_{y1}$. Also in the above solution, $\chi = (k_\xi\xi + k_\eta\eta - \Omega\tau)$, where $\Omega = \frac{6D^2}{25E} + F$ is the frequency of nonlinear structure, $k_\xi = k\cos\varphi$ and $k_\eta = k\sin\varphi$. The solution Eq. (31) of KPB equation (30) is for fast and slow modes of magnetosonic waves and valid for $k_\xi > k_\eta$ only as the stretched variable ξ is of lower order than the coordinate η given in Eq. (22). We note that the structure of the KP equation (30) is the same in the current manuscript and in Maxwellian plasma, however, the only difference is in the definition of $\beta^{'}$ which contains all the nonthermal features, and in the Maxwellian limit $\beta^{'}\rightarrow\beta$ [1,10].

Numerical solution

In this section, we plot the solution (Eq.(31)) of KPB equation for different values of spectral indices Q, (r,q) and kinematic viscosity ν. Fig. 3 depicts the shock profiles of FM and SM magnetosonic wave for different distributions. Fig. 3(a) and (b) represent the FM rarefactive and SM compressive shock profiles, respectively for $Q < 1$ and $r < 0$. We can see that the strength and steepness of FM shock profile is maximum for (r,q)-distribution ($r = -0.4, q = 5$) and least for Maxwellian whereas the strength and steepness of SM shock profile is maximum for Maxwellian and least for (r,q)-distribution ($r = -0.4, q = 5$). A comparison of Fig. 3(a) and 3(b) shows that the non-Maxwellian FM shocks are steeper than the SM shocks but have less shock strength. Fig. 3(c) and 3 (d) represent the FM rarefactive and SM compressive shock profiles, respectively for $Q > 1$ and $r > 0$. We can see that strength and steepness of FM shock profile are maximum for κ-distribution ($\kappa = 2$) and least for (r,q)-distribution ($r = 4, q = 2$) whereas strength and steepness of SM

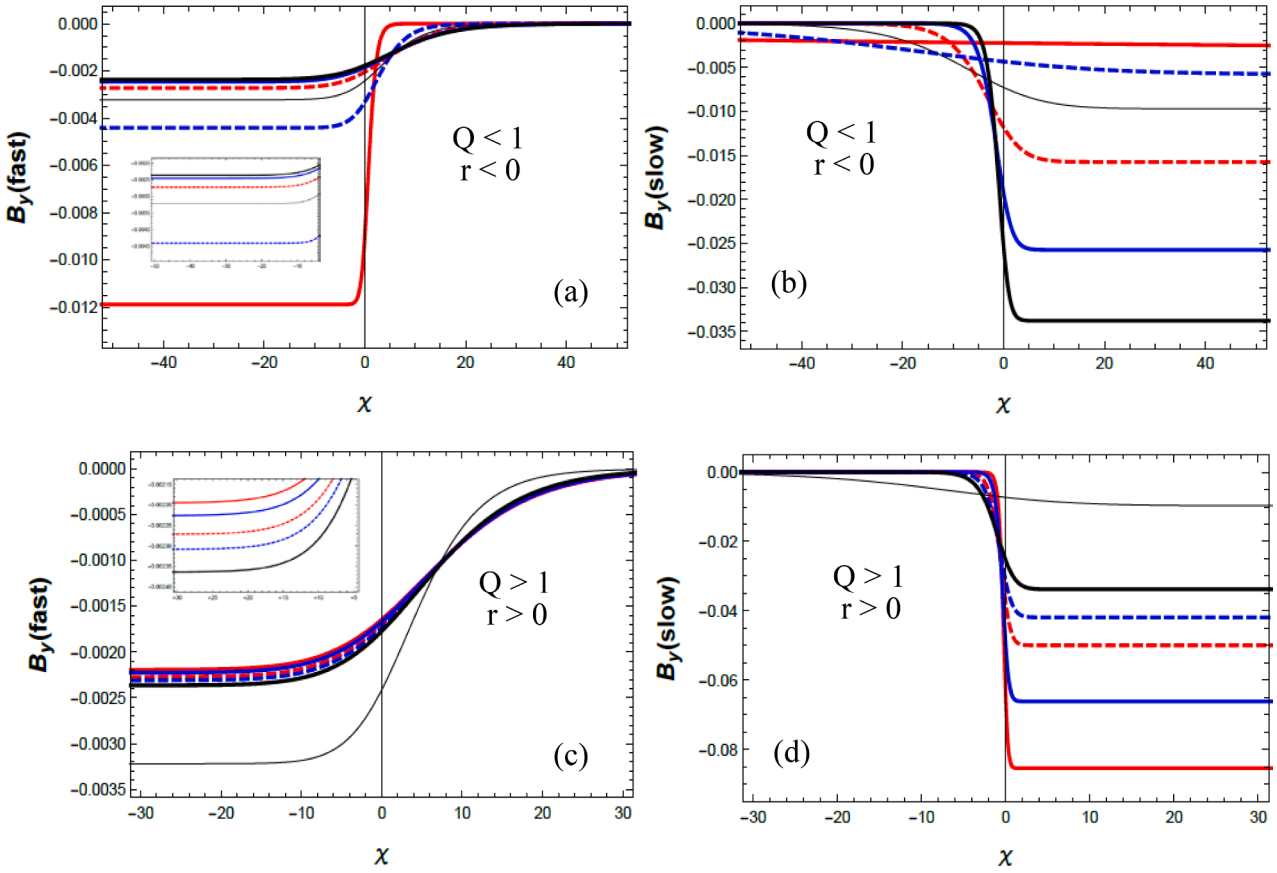

Fig. 3. (a) and (b) depict the fast mode rarefactive and slow mode compressive shock profiles, respectively, when $Q = 0.65$ (dashed blue line), $Q = 0.9$ (solid blue line), $r = -0.1, q = 5$ (dashed red line), $r = -0.4, q = 5$ (solid red line). (c) and (d) depict the fast mode rarefactive and slow mode compressive shock profiles, respectively, when $Q = 1.1$ (dashed blue line), $Q = 1.4$ (solid blue line), $r = 1, q = 2$ (dashed red line), $r = 4, q = 2$ (solid red line). In Fig. 3(a)-(d), $\nu = 0.02$, $\theta = 80^o$, thin black line represents kappa distribution ($\kappa = 2$) and bold black line represents Maxwellian distribution. (For interpretation of the references to colour in this figure legend, the reader is referred to the web version of this article.)

shock profile are maximum for (r,q)-distribution ($r = 4, q = 2$) and least for κ-distribution ($\kappa = 2$). Comparison of Fig. 3(c) and 3(d) shows that the SM shocks are much steeper and have more shock strength than the FM shocks.

Fig. 4 depicts the shock strength for different values of spectral indices $r < 0$, $Q < 1$ and kinematic viscosity ν but for a fixed value of χ. Fig. 4(a) and (b) portray the shock strength of FM and SM shock profiles, respectively, for $r < 0$. In Fig. 4(a), we can see that shock strength increases with ν, however, it increases much faster with ν when the distribution becomes more spiky, i.e.$r\rightarrow -0.4$ than it becomes less spiky, i.e.$r\rightarrow -0.1$. In Fig. 4(b), we can see that shock strength increases with ν, however, it increases much faster with ν when the distribution becomes less spiky, i.e.$r\rightarrow -0.1$ than it becomes more spiky, i.e.$r\rightarrow -0.4$. Fig. 4(c) and (d) portray the shock strengths of FM and SM shock profiles, respectively, for $Q < 1$. In Fig. 4(c), we can see that shock strength increases with ν, however, it increases much faster when the distribution contains high energy tail, i.e.$Q\rightarrow 0.64$ than the distribution when it tends to become Maxwellian, i.e.$Q\rightarrow 1$. In Fig. 4(d), we can see that shock strength increases with ν, however, it increases much faster when the distribution tends to become Maxwellian, i.e.$Q\rightarrow 1$ than the distribution when it contains high energy tail, i.e.$Q\rightarrow 0.64$. Comparison of Fig. 4(a) and 4(c) shows that the FM shock strength is higher for (r,q)-distribution than for Q-distribution for the same values of ν, however, for Fig. 4(b) and 4(d), SM shock strength is higher for Q-distribution than for (r,q)-distribution for the same values of ν. The shaded areas in Fig. 4 represent the values for which the solution becomes non-physical, i.e. $|B_{y1}| > 1$. It is also noted that as the viscosity increases, the amplitude of the soliton increases but the width of the shock front decreases which is evident in Fig. 3.

Fig. 5 depicts the shock strength of the shock profiles for different values of spectral indices $r > 0$, $Q > 1$ and kinematic viscosity ν but for fixed value of χ. Fig. 5(a) and 5(b) portray the shock strength of FM and SM shock profiles, respectively, for $r > 0$. We can see that shock strength increases with ν for FM (Fig. 5(a)) as well as for SM (Fig. 5(b)), however, it increases much faster with ν for SM when the distribution exhibits conspicuous shoulders, i.e.$r\rightarrow 4$ (Fig. 5(b)). We can also note that shock strength remains almost the same for the change in r (Fig. 5(a)). Fig. 5(c) and (d) portray the shock strength of FM and SM shock profiles, respectively, for $Q > 1$. We can see that shock strength increases with ν for FM (Fig. 5(c)) as well as for SM (Fig. 5(d)), however, it increases much faster with ν for SM when the distribution exhibits a broader Gaussian peak with a smaller number of high energy particles as compared to Maxwellian, i.e.$Q\rightarrow 1.4$ (Fig. 5(d)). It can also be noted that shock strength for FM almost remains the same for the change in Q (Fig. 5(c)). Comparison of Fig. 5(a) and 5(c) shows that the FM shock strength is almost the same for (r,q)- as well as for Q-distributions for the same values of ν, however, for Fig. 5(b) and 5(d) tells us that SM shock strength is lower for Q-distribution than for (r,q)-distribution for the same values of ν. Again it can be noted that as the viscosity increases, the amplitude of the soliton increases but the width of the shock front decreases which is evident in Fig. 3.

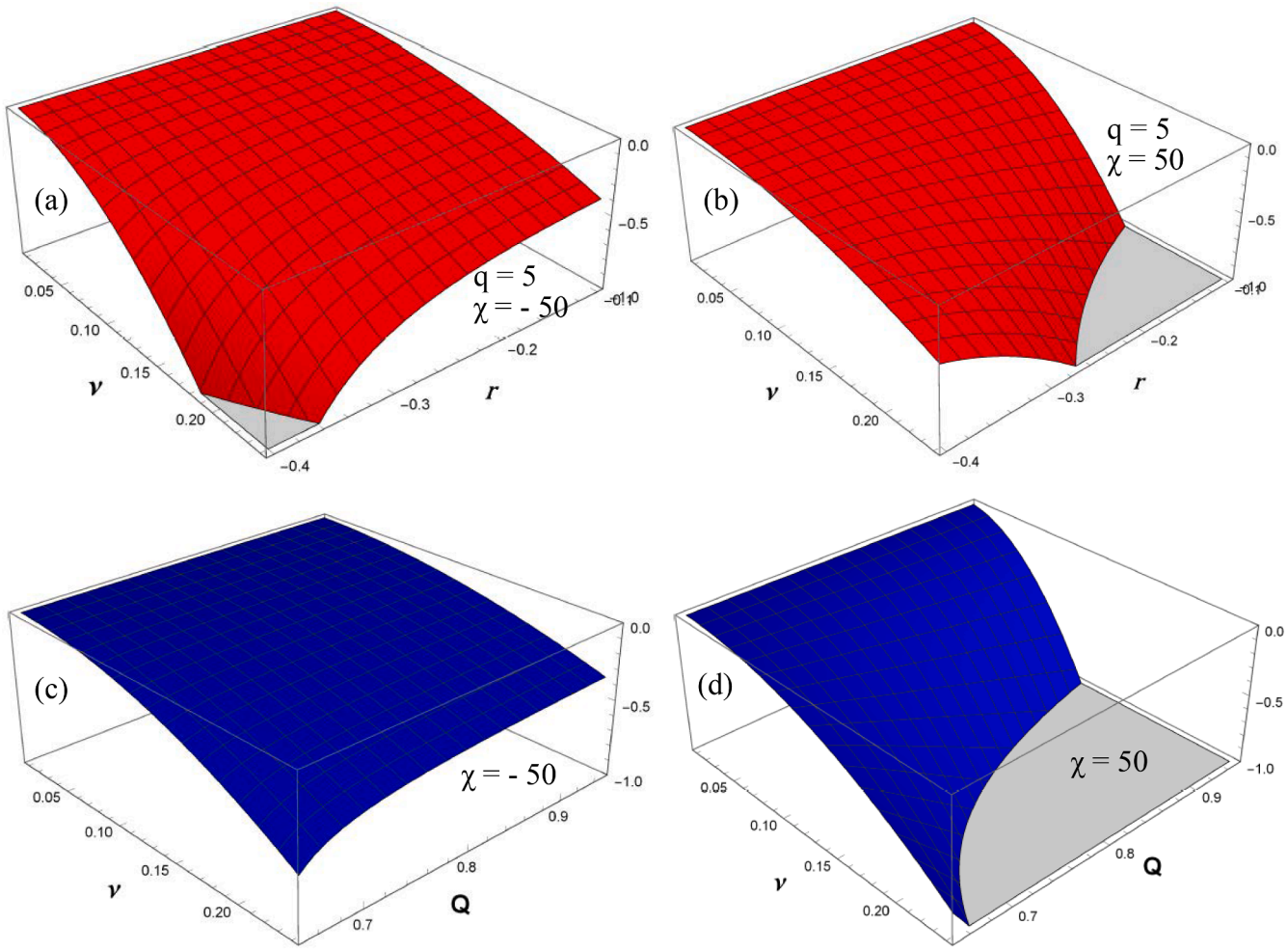

Fig. 4. (a) and (b) depict the variation of shock strength of fast mode rarefactive and slow mode compressive shock profiles for (r,q)-distribution, respectively, for different values of negative r and ν but fixed value of χ. (c) and (d) depict the variation of shock strength of fast mode rarefactive and slow mode compressive shock profiles for non-extensive Q-distribution, respectively, for different values of $Q < 1$ and ν but fixed value of χ. In Fig. 4(a)-(d), $\theta = 80^o$.

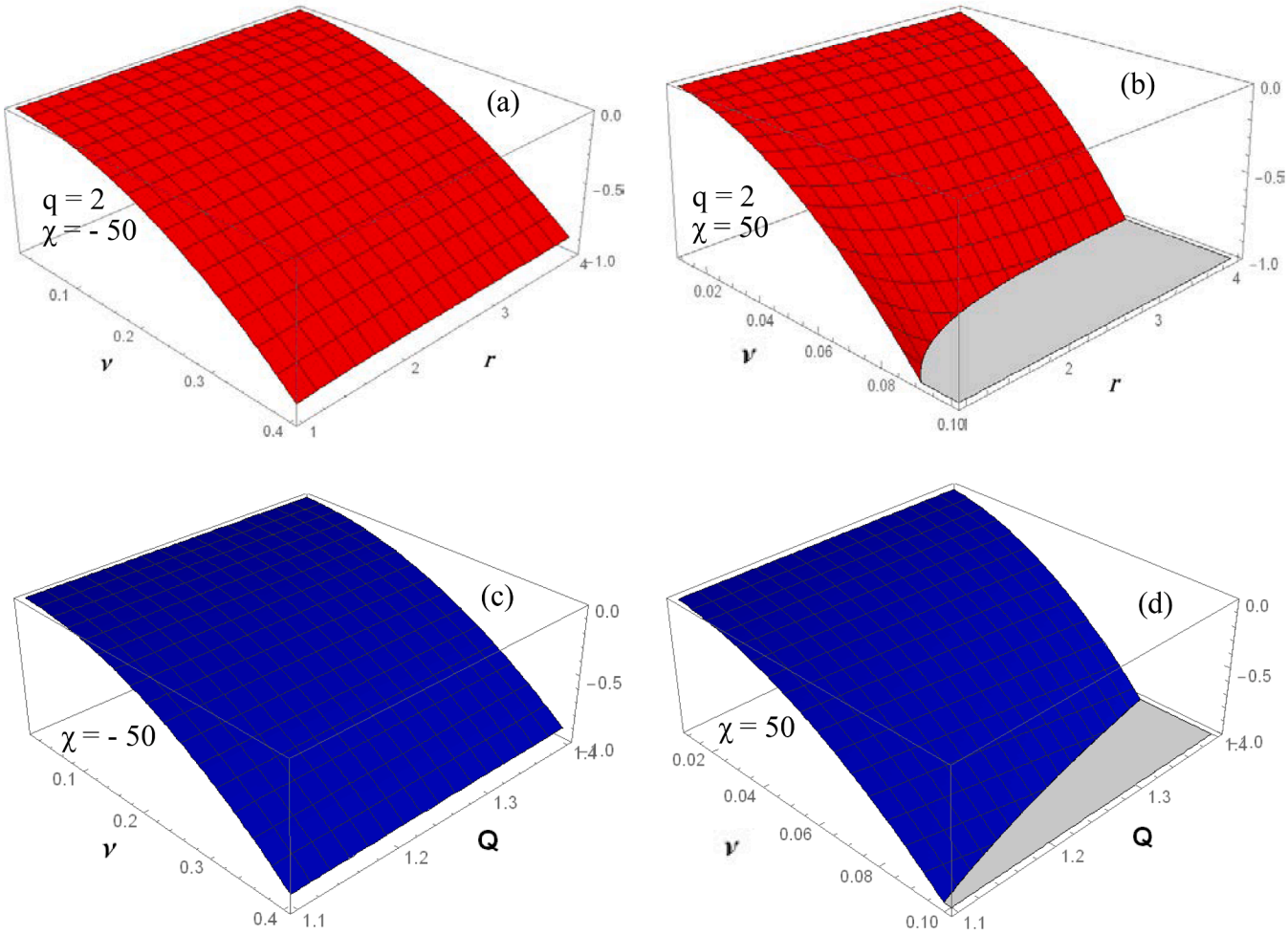

Fig. 5. (a) and (b) depict the variation of shock strength of fast mode rarefactive and slow mode compressive shock profiles for (r,q)-distribution, respectively, for different values of positive r and ν but fixed value of χ. (c) and (d) depict the variation of shock strength of fast mode rarefactive and slow mode compressive shock profiles for non-extensive Q-distribution, respectively, for different values of $Q > 1$ and ν but fixed value of χ. In Fig. 5(a)-(d), $\theta = 80^{\circ}$.

Summary and conclusion

We derived the LDR and KPB equation for slow and fast magnetosonic wave modes in nonthermal plasmas. Fro $Q < 1$ and $r < 0$, linear phase velocity for FM as well as for SM remains highest for (r,q)-distribution showing maximum peak at low energies and least for the Maxwellian. For $Q > 1$ and $r > 0$, the linear phase velocity for both fast and slow modes is highest for κ-distribution exhibiting high energy tail and maximum peak at low energies and least for (r,q)-distribution exhibiting flat top or broader shoulders at low energies. For the nonlinear propagation, when $Q < 1$ and $r < 0$, we found that the strength and steepness of FM shock profile is maximum for (r,q)-distribution exhibiting spiky nature at low energies and least for the Maxwellian whereas strength and steepness of SM shock profile is maximum for the Maxwellian and least for (r,q)-distribution having spiky nature at low energies. For $Q > 1$ and $r > 0$, the strength and steepness of FM shock profile is maximum for κ-distribution exhibiting maximum peak at low energies as well as high energy tail and least for (r,q)-distribution having flat top at low energies whereas strength and steepness of SM shock profile is maximum for (r,q)-distribution with flat top and least for κ-distribution. The dependence of shock strength on the kinematic viscosity ν is also studied. It is found that the shock strength for both the fast and slow modes increases with the increase in ν for all the distributions.

This paper presented the investigations on the obliquely propagating fast and slow magnetosonic wave modes in a hot nonthermal plasma by incorporating the modified temperatures derived from non-extensive Q-distribution, (r,q)-distribution and limiting forms of (r,q)-distribution, i.e. kappa and Maxwellian distributions. For the case of $Q < 1$ and $r < 0$, we found that low energy particles are responsible for the increase in the FM as well as SM linear phase velocities whereas for the case of $Q > 1$ and $r > 0$, high energy particles are responsible for the increase in the FM as well as SM linear phase velocities. For the nonlinear propagation, we found that distribution with both the peak at low energies as well as high energy tail are responsible for the increase in steepness and strength of FM shock profile, however, for the SM shock profiles a distribution with more low energy particles having broader shoulders or Gaussian peak is responsible for the increase in steepness and strength. We also found that the shock amplitude increases with the kinematic viscosity for all distributions. We note here that the main aim of this manuscript is to investigate the effect of nonthermal distribution functions on the propagation of slow and fast mode shock structures. Our numerical results are general since we have used the normalized parameters, so we can apply our results to any region of space and astrophysical plasmas. For example, if we consider the observations of magnetosonic waves near the Earth's magnetic equatorial plane, for which $B_0 = 10nT$, $n_0 = 0.25cm^{-3}$ and $\beta = 0.5$ [58], the shock strength for fast mode ranges from $0.035nT$ to $0.12nT$ and for slow mode, it ranges from $0.35nT$ to $0.83nT$ when $\nu = 0.02$. By increasing the value of viscosity, shock amplitude can also be increased to match the observational values. We, thus found that linear as well as nonlinear propagation of slow and fast magnetosonic wave modes are significantly altered

in the non-Maxwellian plasmas in which nonthermality is incorporated by taking into account the modified temperatures.

CRediT authorship contribution statement

Navaira Izhar: Conceptualization, Investigation, Methodology, Writing – original draft. **M.N.S. Qureshi:** . **J.K. Shi:** Conceptualization, Investigation, Methodology, Writing – original draft. **H.A. Shah:** Conceptualization, Investigation, Methodology, Writing – original draft.

Declaration of Competing Interest

The authors declare that they have no known competing financial interests or personal relationships that could have appeared to influence the work reported in this paper.

Data availability

No data was used for the research described in the article.

Acknowledgment

This research was supported by the Higher Education Commission (HEC), Pakistan Project No. 7558/Punjab/NRPU/R&D/HEC/2017, National Natural Science Foundation of China (42074201), and the Specialized Research Fund for State Key Laboratory in China.

References

[1] Shah HA, Bruno R. Oblique propagation of nonlinear magnetosonic waves. J Plasma Phys 1987;37(1):143–8.
[2] Boardsen SA, Gallagher DL, Gurnett DA, Peterson WK, Green JL. Funnel-shaped low-frequency equatorial waves. J Geophys Res 1992;97(14):967–76.
[3] Horne RB, Wheeler GV, Alleyne HSCK. Proton and electron heating by radially propagating fast magnetosonic waves. J Geophys Res 2000;105(27):597–610.
[4] Meredith NP, Horne RB, Anderson RR. Survey of magnetosonic waves and proton ring distributions in the Earth's inner magnetosphere. J Geophys Res 2008;113 (A6):A06213.
[5] Ma Q, Li W, Chen L, Thorne RM, Kletzing CA, Kurth WS. The trapping of equatorial magnetosonic waves in the Earth's outer plasmasphere. Geophys Res Lett 2014;41 (18):6307–13.
[6] Yang Z, Liu YD, Richardson JD, Lu Q, Huang C, Wang R. Impact of pickup ions on the shock front nonstationarity and energy dissipation of the heliospheric termination shock: Two-dimensional full particle simulations and comparison with Voyager 2 observations. Astrophys J 2015;809(1):28.
[7] Santolík O, Parrot M, Nemec F. Propagation of equatorial noise to low altitudes: Decoupling from the magnetosonic mode. Geophys Res Lett 2016;43(13): 6694–704.
[8] Su Z, Wang G, Liu N, Zheng H, Wang Y, Wang S. Direct observation of generation and propagation of magnetosonic waves following substorm injection. Geophys Res Lett 2017;44(15):7587–97.
[9] Yuan Z, Yu X, Huang S, Wang D, Funsten HO. In situ observations of magnetosonic waves modulated by background plasma density. Geophys Res Lett 2017;44(15): 7628–33.
[10] Mushtaq A, Shah HA. Effect of positron concentration, ion temperature, and plasma β value on linear and nonlinear two-dimensional magnetosonic waves in electron-positron-ion plasma. Phys Plasmas 2005;12:012301.
[11] Chakrborty D, Das KP. Evolution of nonlinear magnetosonic waves propagating obliquely to an external magnetic field in a collisionless plasma. J Plasma Phys 2001;64(3):211–26.
[12] Mushtaq A, Qamar A. Parametric studies of nonlinear magnetosonic waves in two-dimensional quantum magnetoplasmas. Phys Plasmas 2009;16:022301.
[13] Tanenbaum BS, Mintzer D. Wave propagation in a partly ionized gas. Phys Fluids 1962;5(10):1226–37.
[14] Zavershinskii D, Kolotkov D, Riashchikov D, Molevich N. Mixed properties of slow magnetosonic waves in a plasma with heating/cooling misbalance. Sol Phys 2021; 296:96.
[15] Demiray H, Abdikian A. Analysis of periodic and solitary waves in a magnetosonic quantum dusty plasma. Indian J Phys 2021;95(6):1255–61.
[16] El-Awady EI, El-Tantawy SA, Abdikian A. Dissipative cylindrical magnetosonic solitary waves in a magnetized quantum dusty plasma. Romanian Rep Phys 2019; 71(2):105.
[17] Kawahara TJ. Weak nonlinear magneto-acoustic waves in a cold plasma in the presence of effective electron-ion collisions. Phys Soc Japan 1970;28(5):1321–9.
[18] Janaki MS, Som BK, Dasgupta B, Gupta MR. K-P Burgers equation for the decay of solitary magnetosonic waves propagating obliquely. J Phys Soc Japan 1991;60(9): 2977–84.
[19] Janaki MS, Dasgupta B, Gupta MR, Som BK. Magnetosonic shock waves propagating obliquely in a warm collisional plasma. Phys Scr 1991;44(2):203–7.
[20] Pandey BP, Vranjes J. The solitary wave propagation in a collisional dusty plasma. Phys Plasmas 2008;15(8):083701.
[21] Ghosh UN, Mandal PK, Chatterjee P. The roles of nonextensivity and dust concentration as bifurcation parameters in dust-ion acoustic traveling waves in magnetized dusty plasma. Phys Plasmas 2014;21(3):033706.
[22] Hussain S, Hasnain H. Magnetosonic wave in pari-ion electron collisional plasmas. Phys Plasmas 2017;24(3):032106.
[23] Akhtar N, Hussain S, Mahmood S. Nonlinear propagation of fast and slow magnetosonic waves in collisional plasmas. Cont Plasma Phys 2021;61(5): e202000210.
[24] Vasyliunas VM. A survey of low-energy electrons in the evening sector of the magnetosphere with OGO 1 and OGO 3. J Geophys Res 1968;73(9):2839–84.
[25] Feldman W, Bame S, Gary S, Gosling S, McComas D, Thomsen M, et al. Electron heating within the Earth's bow shock. Phys Rev Lett 1982;49(3):199–201.
[26] Summers D, Thorne RM. The modified plasma dispersion function. Phys Fluids B 1991;3(8):1835–47.
[27] Pierrard V, Lemaire J. Lorentzian ion exosphere model. J Geophys Res 1996;101 (A4):7923–34.
[28] Qureshi MNS, Shah HA, Murtaza G, Schwartz SJ, Mahmood F. Parallel propagating electromagnetic modes with generalized (*r, q*) distribution function. Phys Plasmas 2004;11(8):3819–29.
[29] Qureshi MNS, Shi JK, Ma SZ. Influence of generalized (r, q) distribution function on electrostatic waves. Commun Theo Phys 2006;45(3):550–4.
[30] Kiran Z, Shah HA, Qureshi MNS, Murtaza G. Parallel proton heating in solar wind using generalized (r, q) distribution function. Solar Phys 2006;236:167–82.
[31] Sehar Sumbul, Qureshi MNS, Shah H A. Electron acoustic instability in four component space plasmas with observed generalized (*r, q*) distribution function. AIP Adv 2019;9:025315.
[32] Qureshi MNS, Warda N, Masood W, Yoon PH, Shah HA, Schwartz SJ. Terrestrial lion roars and non-Maxwellian distribution. J Geophys Res 2014;119:10059–67.
[33] Khalid Saba, Qureshi MNS, Masood W. Nonlinear kinetic Alfven waves in space plasmas with generalized (r,q) distribution. Astrophys Space Sci 2018;363:216.
[34] Shah KH, Qureshi MNS, Masood W, Shah HA. Electron acoustic nonlinear structures in planetary magnetospheres. Phys Plasmas 2018;25:042303.
[35] Shah KH, Qureshi MNS, Masood W. Alternative explanation for the density depletions observed by Freja and Viking satellites. AIP Adv 2018;8:085010.
[36] Khalid Saba, Qureshi MNS, Masood W. Compressive and rarefactive solitary structures of coupled kinetic Alfven-acoustic waves in non-Maxwellian space plasmas. Phys Plasmas 2019;26:092114.
[37] Khalid Saba, Qureshi MNS, Masood W. Alfvenic perturbations with finite Larmor radius effect in non-Maxwellian electron-positron-ion plasmas. AIP Adv 2019;10: 025002.
[38] Qureshi MNS, Shah KH, Shi JK, Masood W, Shah HA. Investigations of cubic non-linearity-driven electrostatic structures in the presence of double spectral index distribution function. Contrib Plasma Phys 2019;60:e201900065.
[39] Niknam AR, Roozbahani H, Hashemzadeh M, Komaizi D. Particle in cell simulations of Buneman instability of a current-driven plasma with q-nonextensive electron velocity distribution. Phys Plasmas 2014;21(9):092307.
[40] Aman-ur-Rehman AM, Shan AA, Majeed T. Kinetic theory of ion acoustic waves in a q-nonextensive distributed ions and electrons plasma. Phys A 2018;506:938–48.
[41] Asserghine A, El KM, Chatei H. Investigation of magnetized plasma sheath in the presence of q-nonextensive electrons and negative ions. Mater Today: Proc 2020;24 (1):24–8.
[42] Lin FJ, Liao J-J, Zhu Y. Ion-acoustic solitary waves in a q-nonextensive plasma. Chin Astron Astrophy 2015;39(3):295–306.
[43] Silva R, Alcaniz JS. Negative heat capacity and non-extensive kinetic theory. Phys Letts A 2003;313(5–6):393–6.
[44] Heerikhuisen J, Pogorelov NV, Florinski V, Zank GP, Roux JA. The effects of a κ-distribution in the heliosheath on the global heliosphere and ENA flux at 1 AU. Astrophys J 2008;682(1):679–89.
[45] Fahr HJ, Siewert M. The multi-fluid pressures downstream of the solar wind termination shock. A & A 2013;558:A41.
[46] Livadiotis G. Kappa distributions: Theory and applications in space plasmas 2017: Elsevier.
[47] Shaikh S, Khan A, Bhatia PK. Thermally conducting partially ionized plasma in a variable magnetic field. Contrib Plasma Phys 2007;47(3):147–56.
[48] Sharifian M, Sharifinejad HR, Zarandi MB, Niknam AR. Effect of q-non-extensive distribution of electrons on the plasma sheath floating potential. J Plasma Phys 2014;80(4):607–18.
[49] Liu Y, Shi ZF, Han Y, Dai B. Properties of solitary kinetic Alfven wave in a plasma with non-extensive electrons. Phys Plasmas 2015;22(3):032103.
[50] Vinas AF, Moya PS, Navarro RE, Valdivia JA, Araneda JA, Munoz VJ. Electromagnetic fluctuations of the whistler-cyclotron and firehose instabilities in a Maxwellian and Tsallis-kappa-like plasma. Geophys Res Space Physics 2015;120 (5):3307–17.
[51] Washimi H, Taniuti T. Propagation of ion-acoustic solitary waves of small amplitude. Phys Rev Lett 1966;17(19):996–8.
[52] Abdikian A, Tamang J, Saha A. Supernonlinear wave and multistability in magneto-rotating plasma with (r, q) distributed electrons. Phys Scr 2021;96(9): 095605.
[53] Abdikian A, Tamang J, Saha A. Investigations of supernonlinear and nonlinear ion-acoustic waves in a magnetized electron-ion plasma with generalized (r, q) distributed electrons. Waves Random Complex Media 2021. https://doi.org/10.1080/17455030.2021.1965242.

[54] Malfliet W. Solitary wave solutions of nonlinear wave equations. Am J Phys 1992; 60(7):650–4.
[55] Malfliet W. The tanh method: a tool for solving certain classes of nonlinear evolution and wave equations. J Comput Appl Math 2004;164–165(7):529–41.
[56] Raut S, Roy A, Mondal KK, Chatterjee P, Chadha NM. Non-stationary solitary wave solution for damped forced Kadomstev-Petviashvili equation in a magnetized dusty plasma with q-nonextensive velocity distributed electron. Int J Appl Comput Math 2021;7:223. https://doi.org/10.1007/s40819-021-01168-2.
[57] Masood W, Jehan N, Mirza AM. A new equation in two dimensional fast magnetoacoustic shock waves in electron-positron-ion plasma. Phys Plasmas 2010; 17(3):032314.
[58] Huang SY, Deng D, Yuan ZG, Jiang K, Li JX, Deng XH, et al. First observations of magnetosonic waves with nonlinear harmonics. J Geophys Res Space Phys 2020; 125(6):e2019JA027724.